Tuning Infrared Emissivity of Graphene Aerogel Through Ion Intercalation

Zekai Weng,[1] Haibo Ke,[1] Xiaoxiao Guo,[1] Shujian Cheng,[1] Tong Lin,[1] Wenlian Peng,[2] Mengyan Dai,[2] Weiwei Cai,[1] Yufeng Zhang,[1,*] and Xue-ao Zhang[1,3,†]

[1] *College of Physical Science and Technology, Xiamen University, Xiamen, 361005, China*
[2] *Institute of Chemical Defense, Academy of Military Science, Beijing, 102205, China*
[3] *Jiujiang Research Institute of Xiamen University, Jiujiang, 360404, China*

(Received 27 June 2022; revised 11 August 2022; accepted 12 August 2022; published 1 September 2022)

Dynamically modulating the infrared emissivity of materials is of great importance in various applications (e.g., thermal camouflage and radiative cooling). Even though graphene-based materials (such as multilayer graphene, MLG) have shown great potential in active control of emissivity, the device lifetime is rather short, while low-cost large-scale production is difficult to achieve. Herein, graphene aerogels (GAs) with high porosity are prepared by a simple hydrothermal method, and used as electrode in an infrared emissivity modulator with a sandwiched structure. It is demonstrated that the emissivity of GA can be tuned through ion intercalation by electrostatic gating. The modulation depth of GA is comparable to that of MLG, but device lifetime is much longer. This is likely due to the porous structure of GA formed by a continuous three-dimensional MLG network, which makes it easier for ion transport, while allowing effective charge transfer from anions adsorbed on or intercalated into MLG to carbons. Due to a change in surface roughness of GA upon compressing, the emissivity of GA can be further tuned by compressive strain, which provides additional freedom in control of emissivity. The observations offer a promising avenue for the preparation of large-scale emissivity modulators at low cost, which is beneficial for practical applications.

DOI: 10.1103/PhysRevApplied.18.034003

I. INTRODUCTION

Controlling the infrared emissivity of materials has attracted great attention, due to its potential in various applications, such as radiative cooling [1,2] and thermal camouflage [3]. By tuning the structure of a material, for example poly(vinylidene fluoride-co-hexafluoropropene) [4] and cellulose nanofibers [5], it is possible to achieve continuous subambient cooling even during daytime. However, this lacks the capability to adjust the emissivity dynamically. Several mechanisms, such as phase transition (e.g., VO_2 [6], $Ge_2Sb_2Te_5$ [7]) and strain engineering [8,9], have been proposed for active control of emissivity. Nevertheless, there are still several challenges (e.g., small operation temperature window, slow dynamic response).

Graphene with zero band gap and linear band dispersion [10] can absorb photons in the range from visible light to infrared. Due to the Pauli compulsion principle, the interband and intraband transitions of charge carriers can be reduced by regulating the Fermi level of graphene through optical excitation [11] or doping [3]. Ion intercalation is an effective method to provide a reversible doping for carbon-based material [12]. Recently, it has been demonstrated that the emissivity of graphene-based materials, such as multilayer graphene (MLG), can be tuned reversibly through ion intercalation [13]. However, the device lifetime is rather short (e.g., usually less than 1 h), due to structural damage of MLG induced by chemical reaction between ionic liquids (ILs) and MLG [3] as well as fast ion intercalation processes [14]. Several methods (e.g., using an IL with small molecular size [14]) have been explored to improve the device lifetime, with limited success due to the characteristics of the MLG structure (e.g., weakening van der Waals interaction between graphene layers due to presence of ILs). Furthermore, MLG-based materials must be prepared using sophisticated equipment, such as a chemical vapor deposition system [15], with complicated processes (e.g., deposition on a template followed by etching procedure [16]). Therefore, it is rather difficult to synthesize these materials on a large scale at low cost, hindering their application in emissivity modulation.

Graphene aerogels (GAs), which can be prepared by a simple hydrothermal method, consist of continuous three-dimensional network structures formed by MLG, and possess unique properties, such as high specific surface area and excellent elasticity [17,18]. Furthermore, the thermal properties of GAs can be reversibly tuned by compressive strain [17], which indicates that GAs are resilient to external perturbation. For example, ions can transport in

*yufengzhang@xmu.edu.cn
†xazhang@xmu.edu.cn

a GA without introducing irreversible damage to its structure. Hence, this study investigates the potential of GAs as a functional material in an infrared emissivity modulator. The results suggest that the emissivity of GAs can be tuned by two factors, compressive strain and ion intercalation. The modulation depth of a GA is comparable to that of MLG, but the device lifetime is about five times longer. The observations open a promising avenue for practical applications of the emissivity modulator.

II. EXPERIMENT

Cylindrical GAs each with a height of 0.5 cm and a radius of 1.0 cm are prepared by the hydrothermal method [17]. In short, 45 μl of ethylenediamine and 12 ml of a graphene oxide water dispersion (with a density of 3 mg/mL) are mixed and placed in an autoclave at 180 °C for 2 h. The obtained hydrogel is washed and freeze-dried, followed by an annealing at 3000 °C to form GA. Slices with a thickness of about 600 μm are cut from the cylindrical GA and compressed by a homemade compressor (consisting of two parallel anvils constrained by a linear bearing) with different pressures to obtain samples with compressive strain of 0%, 33%, 60%, 70%, 80%, and 90%, respectively. Note that the strain is quantified by $\Delta D/D$, where D is the original thickness of the sample and ΔD is the change in thickness.

Based on previous work [19], the samples as well as a polished Cu foil (99%, Alfa Aesar Inc.), a Celgard 2325 separator (25 μm thick, polypropylene-polyethylene-polypropylene, Celgard Inc.) and ionic liquids ([HMIm]NTf_2) are used to prepare the infrared emissivity modulator with a sandwiched structure.

The emissivity modulator is laid on a hot plate (V-2020T, VECTECH Inc.) to simulate working temperature, while two thermocouples are used to monitor the temperature of the GA and the ambient temperature. A power source (DP155, MESTEK Inc.) provides a direct-current voltage between two electrodes of the modulator for gating ion intercalation, while a signal generator (Tektronix AFG3101C) is used for cyclic tests. A Tix500 thermal camera (model Ti450, Fluke Inc., spectral range from 7.5 to 14 μm) is deployed to capture the thermal images of the modulators, as shown in Fig. 1(a). Note that the emissivity is set to 1 in the thermal camera, and the temperature of GAs measured by a thermocouple is 69 °C, while the ambient temperature is 25 °C. Furthermore, infrared spectra of MLG are investigated using a Fourier transform infrared spectrometer (IS50, Thermo Fisher Scientific). Meanwhile, the sheet resistance of graphene aerogels is

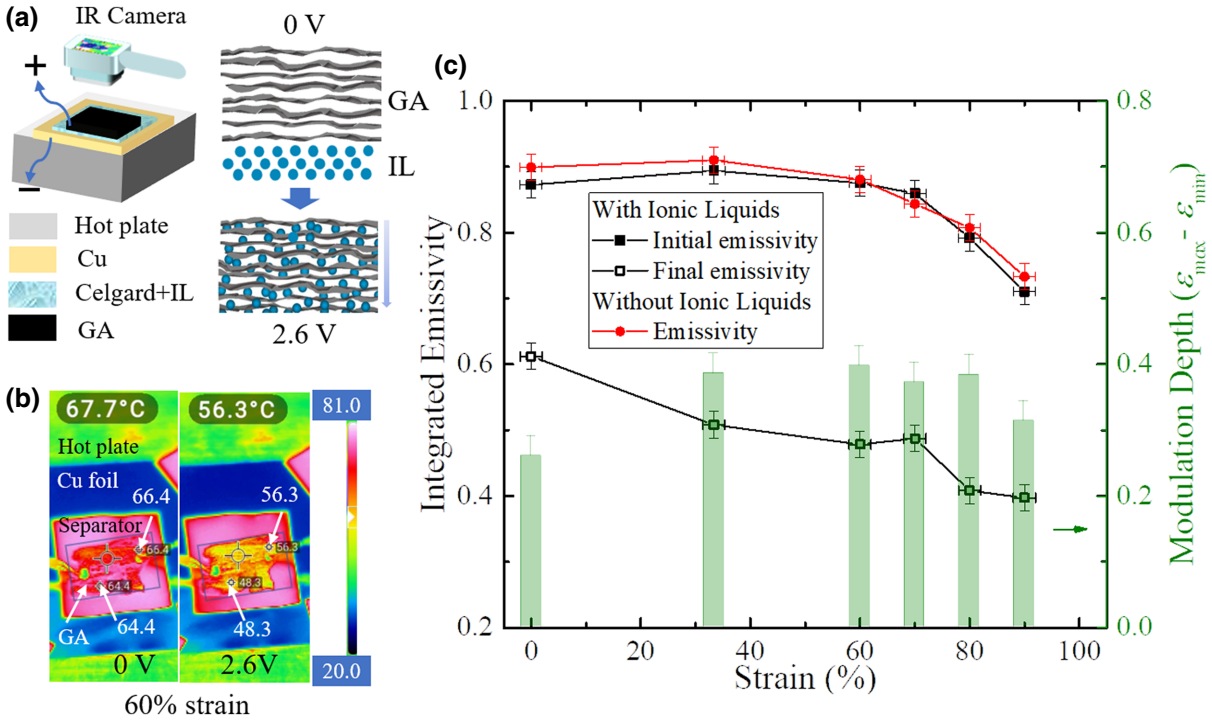

FIG. 1. (a) Schematic diagram of the infrared emissivity modulator, in which the separator and IL are sandwiched by Cu foil and GA. After applying a bias, ions in IL are intercalated into GA. (b) Thermal images of GA with 60% strain before (left panel) and after (right panel) applying a bias voltage. The color bar indicates the reddish area is of higher apparent temperature, while the blueish area is of lower temperature. (c) The initial and final emissivity of GA in a modulator with IL, and the modulation depth as a function of strain. For comparison, the initial emissivity of GA without the presence of IL is depicted.

measured by a four-point probe system (HP-504). The electrochemical surface area (ECSA) of GAs is investigated using a potentiostat (CHI660E, CH Instruments, Inc.) in cyclic voltammetry mode.

The GA samples are extracted from the modulators for microscopic analysis. Cross-section structural changes of GA are studied by scanning electron microscopy (SEM) with a Carl Zeiss FE-SEM Sigma HD, while the crystal structures are characterized by x-ray diffraction (XRD) at ambient conditions (MAXima XRD-7000) with a Cu Kα excitation source and Raman spectroscopy (WItec alpha 300RA) using the 488 nm line of an Ar^+ laser. The surface roughness of the samples is measured by laser confocal microscopy (LSM 800, Zeiss Sigma).

III. RESULTS AND DISCUSSION

The infrared emissivity of GA with various uniaxial compressive strains is investigated using a modulator with sandwiched structure (i.e., GA/separator-IL/Cu), as shown in Fig. 1(a). The apparent temperature (T_{IR}) of GA with 60% strain, obtained by a thermal camera, decreases from 67.7 to 56.3 °C after applying a 2.6-V bias voltage, as shown in Fig. 1(b). Similar behaviors are observed for GA with or without strain, as depicted by thermal images (Supplemental Material, Sec. S1 [20]). Note that the change in T_{IR} is not homogeneous in space, which is likely due to nonuniformity in surface morphology of the samples. Usually, integrated emissivity (ε), which takes into account overall infrared radiation captured by a thermal camera, is used to quantitatively assess the ability of a material in regulating infrared radiation [15]. This parameter regulates the overall signal received by an infrared sensor, and closely correlates with the performance of a material in practical applications (e.g., thermal camouflage). Generally, the infrared radiation from an object captured by a thermal camera consists of two parts: the emission from the object itself and the background emission reflected by the object. Hence, the value of ε is derived as [14]

$$\varepsilon = \frac{T_{IR}^4 - T_0^4}{T_R^4 - T_0^4}, \tag{1}$$

where T_R and T_0 are the real temperature of GA and ambient temperature, respectively. The uncertainty of ε is estimated to be ± 0.02.

Due to the spatial inhomogeneity, the lowest ε of the samples is shown in Fig. 1(c). The initial emissivity of GA (i.e., without a bias voltage) is nearly unchanged (approximately 0.88) when the strain is less than 60%, then quickly drops to 0.71 with a strain of 90%. A set of GAs with the same strains but no ILs is characterized at the same conditions (e.g., with the same T_R and T_0). The results [marked as red dots in Fig. 1(c)] agree well with the results obtained from samples with ILs. This suggests that the change in the initial emissivity is not due to the presence of ILs, but more likely is associated with the strain.

Applying a bias voltage drives ions in the ILs toward the GA, as shown in Fig. 1(a). Some of the anions adsorb on or intercalate into graphene layers in the GA, and transfer charges to carbons in graphene, which greatly increases the charge density of the GA. This results in an increase of Fermi level, which changes the interband and intraband transitions of charge carriers (e.g., electrons) [3]. Therefore, the emissivity of GA decreases upon applying a bias voltage. The charge transfer between anions and carbons also leads to a decrease in the sheet resistance of GA. The change in the sheet resistance grows from 9% to 15% when strain increases from 0% to 70%, but drops to 8% with a further increase in strain (e.g., 90%), as depicted in the Supplemental Material, Sec. S2 [20]. The modulation depth is positively correlated with the decrease of sheet resistance. Similar results have been observed in a modulator using MLG as electrode [13]. Interestingly, the modulation depth (i.e., the difference between the initial and final emissivity) does not monotonically decrease as the strain increases, which is likely due to a change in the ECSA. Nevertheless, the maximum modulation depth (approximately 0.40 with a 60% strain) is comparable to the results obtained with a modulator using the same ILs but MLG as electrode [14], and better than those for freestanding graphene fabric film [16]. As shown in the Supplemental Material, Sec. S3 [20], the emissivity of GA can be reversibly tuned by adjusting the bias voltage, and maintained at a value not greater than the lowest value plus 0.1 for about 2 h, which is nearly five times longer than that of a modulator using MLG (e.g., approximately 26 min [14]). Meanwhile, the emissivity of MLG-based modulator ion intercalation can be determined at a temperature from 300 to 340 K, with a dynamic response rate of 0.15 s^{-1} (e.g., the emissivity changes from 0.55 to 0.1 in 3 s) [3,19,21]. Since the operation temperature window in this type of modulator is mainly determined by ionic liquids and separator, the GA-based modulator can effectively tune infrared emissivity in a similar temperature window. However, it should be pointed out that the dynamic response rate of GA is much slower than that of MLG, which is likely due to larger thickness and porosity of GA. Hence, GA might not be ideal for applications that require fast-dynamic response. Nevertheless, using GA as electrode provides a better performance than using MLG, while offering the possibility for producing a large-scale modulator at low cost.

To shed light on the change in the initial emissivity, the morphology and surface roughness of GA are investigated by laser confocal microscopy. The results shown in Fig. 2(a) suggest that the surface roughness of GA decreases with increasing strain. The root-mean-square roughness (Sq) of GA quickly drops from 58 to 26 μm, when the strain increases to 60%, then reaches a plateau

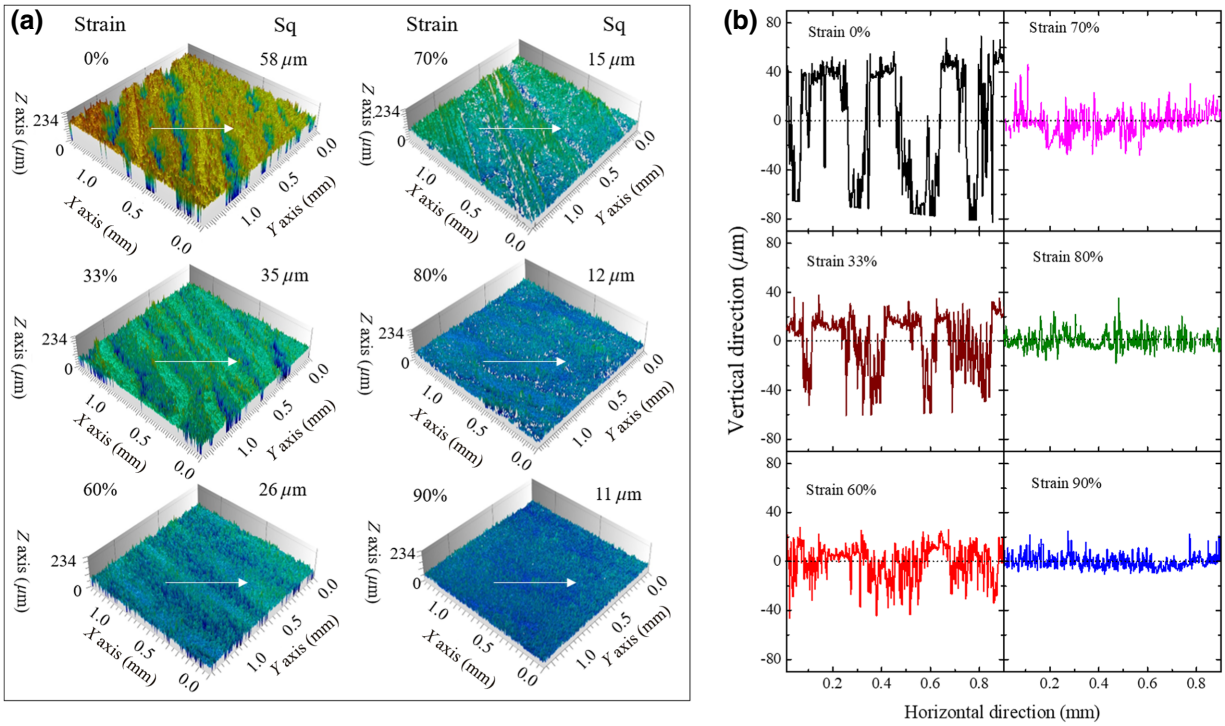

FIG. 2. (a) Surface morphology of GA with 0%, 33%, 60%, 70%, 80%, and 90% strain. The roughness of samples is assessed in terms of the root-mean-square value (Sq). (b) Linear profiles of the corresponding GA samples extracted from the marked arrows.

of around 11 μm with a strain larger than 80%. Note that the uncertainty of Sq is ± 2 μm. This agrees well with the change in the initial emissivity, e.g., from 0.88 to 0.71 as the strain increases from 60% to 90%. It has been reported that 10-μm-pitch crumpled graphene offers midinfrared emissivity control at wavelengths of 7–19 μm [8]. Therefore, it is not surprising that significant modulation of the emissivity derived from the signal of the thermal camera is only observed with strain larger than 60%.

To further analyze the change in surface structure, the linear profiles (marked as white arrows) of corresponding samples are depicted in Fig. 2(b). Clearly, some areas of the sample are smoother than others. For example, if the whole profile of GA with 60% strain is evenly divided into 100 pieces, the standard deviation of height for each piece varies between 4 and 16 μm. This likely originates from the sample preparation (e.g., cutting a slice of GA and compressing it to a set value), and contributes to the spatial inhomogeneity of T_{IR} observed in Fig. 1(b). Further research is underway to improve the spatial homogeneity in tuning emissivity by optimizing the sample preparation procedure.

The cross-section structures of the samples are investigated by SEM, as shown in Fig. 3(a). GA consists of a continuous three-dimensional structure formed by MLG, which is consistent with our previous report [17]. Qualitatively, the porous structure of GA gradually becomes a layer structure with increasing strain. The porosity of samples, estimated by a false-color mapping (e.g., taking all pixels with grayness less than 100 as the area occupied by pores, as detailed in the Supplemental Material, Sec. S4 [20]), changes from 56% to 20%, while the average pore diameter changes from approximately 50 to approximately 10 μm, respectively. This indicates that the resisting force induced by capillary pressure increases with increasing strain and could make it harder for ILs to transport in GA. Furthermore, excessive strain might lead to structural change that prevents ILs from accessing some internal space in GA.

The surface area of GA is further determined with an electrochemical measurement of the double layer capacitance (C_{dl}). If assuming that the capacitance of an ideal flat surface of the electrode (GA) with the same ILs is a constant (C_S), ECSA can be derived as [22]

$$\mathrm{ECSA} = \frac{C_{dl}}{C_S}. \tag{2}$$

Hence, the ECSA of the samples can be revealed using a potentiostat in cyclic voltammetry mode in a narrow non-Faraday reaction potential window [23], as detailed in the Supplemental Material, Sec. S5 [20]. The value of C_{dl} increases from 4.0 μF/cm^2 for GA without strain to 6.5 μF/cm^2 for GA with a 60% strain, but decreases to 4.7 μF/cm^2 when the strain increases to 90%. The change in ECSA shows a strongly positive correlation with the

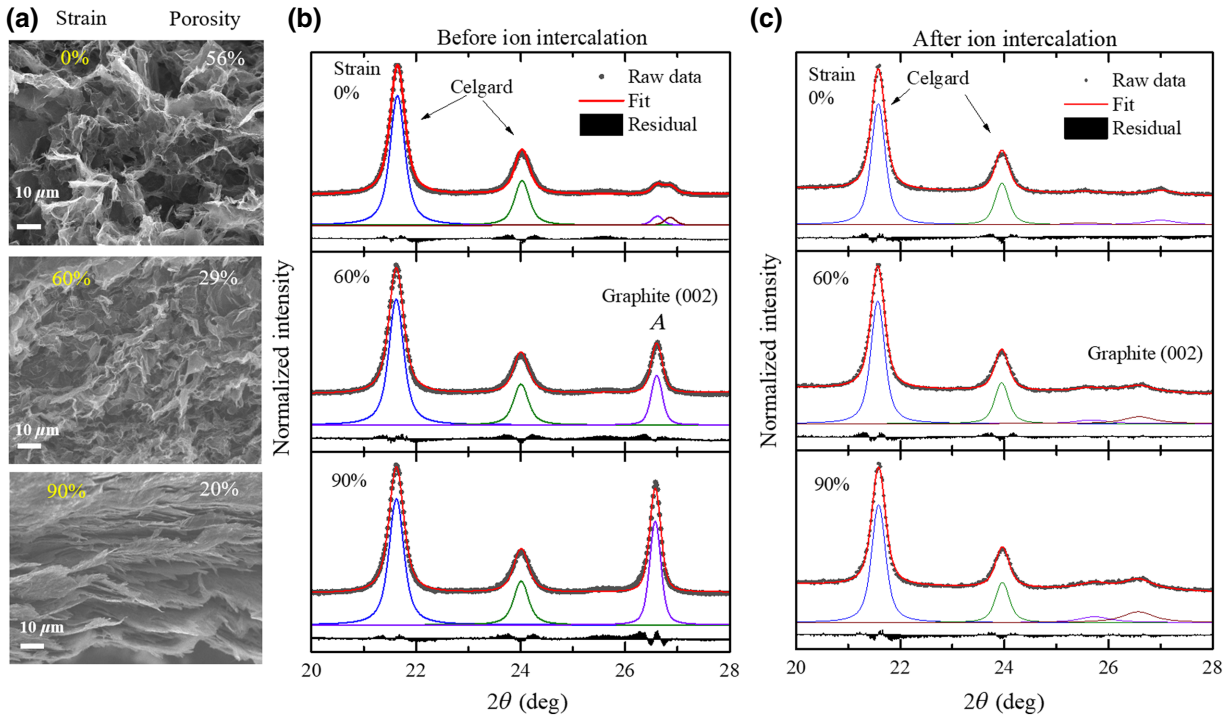

FIG. 3. (a) Cross-section SEM images of GA with 0%, 60%, and 90% strain, while the porosity of each sample is estimated by a MATLAB code based on false-color mapping. XRD patterns of GA with 0%, 60%, and 90% strain (b) before and (c) after ion intercalation, as well as curve fits for the dominant features.

change in modulation depth with a Pearson correlation of 0.99 and two-tailed significance of 7.5×10^{-5}.

Generally, the ECSA represents the area of an electrode that is available for an electrochemical reaction. Hence, it is commonly used to assess catalytic activity of materials [23]. Here, it is correlated with the effective area of GA, which interacts with ionic liquids. A higher value suggests that more internal surface of GA is accessible to ionic liquids, which allows anions to be adsorbed, and therefore provides a better chance for charges to be transferred from ionic liquid to GA. It is reported that the modulation depth is proportional to the amount of transferred charge [24]. Therefore, it is not surprising that a greater ECSA leads to a larger modulation depth. Meanwhile, it was reported in our previous study that the thermal conductivity of GA in the in-plane direction increases with increasing strain (especially for values larger than 80%), which is likely due to more overlapping between adjacent graphene sheets [17]. This suggests that, at high strain level (e.g., 90%), some of the internal area of GA is blocked (i.e., harder to reach for anions in IL), which is also supported by SEM images and decrease of porosity shown in Fig. 3(a). Therefore, the value of ECSA dramatically decreases when the strain is larger than 80%.

To further investigate the structural change in GA after compression and ion intercalation, the XRD patterns of the samples are shown in Figs. 3(b) and 3(c) over a 2θ diffraction range of 20°–28°. Note that all patterns are normalized to the intensity of the feature at 21.6°. Generally, all patterns possess at least three features: two features at 21.6° and 24.1° are from the separator (i.e., Celgard), and feature A at around 26.6° originates from graphite or multilayer graphene (002) [14]. The curve fits suggest that at least two Voigt functions are needed to obtain a reasonable fit for feature A from GA without strain, but only one Voigt function is sufficient for GA with 60% or 90% strain. Meanwhile, the intensity of feature A (I_A) increases from 0.04 for GA without strain to 0.25 for GA with 90% strain. This indicates that the graphene layers stack in a much more ordered manner as the strain increases.

After ion intercalation, I_A of GA with strain dramatically decreases (e.g., from 0.25 to 0.09 for GA with 90% strain), while the full width at half maximum (FWHM) of feature A increases greatly (from 0.26° to 0.72°). However, I_A of GA without strain does not change significantly (e.g., from 0.04 to 0.05). This suggests that introducing ILs damages the stacking order of graphene layers.

However, unlike MLG, there is no significant increase of defects in GA upon ion intercalation. This is evident from the Raman spectra of GAs before and after ion intercalation, as shown in Fig. 4(a). Note that the spectra are normalized to [0, 1] for easier comparison of the change in spectral intensity. The spectra of pristine GA only possess two dominant features, G at 1590 cm^{-1}

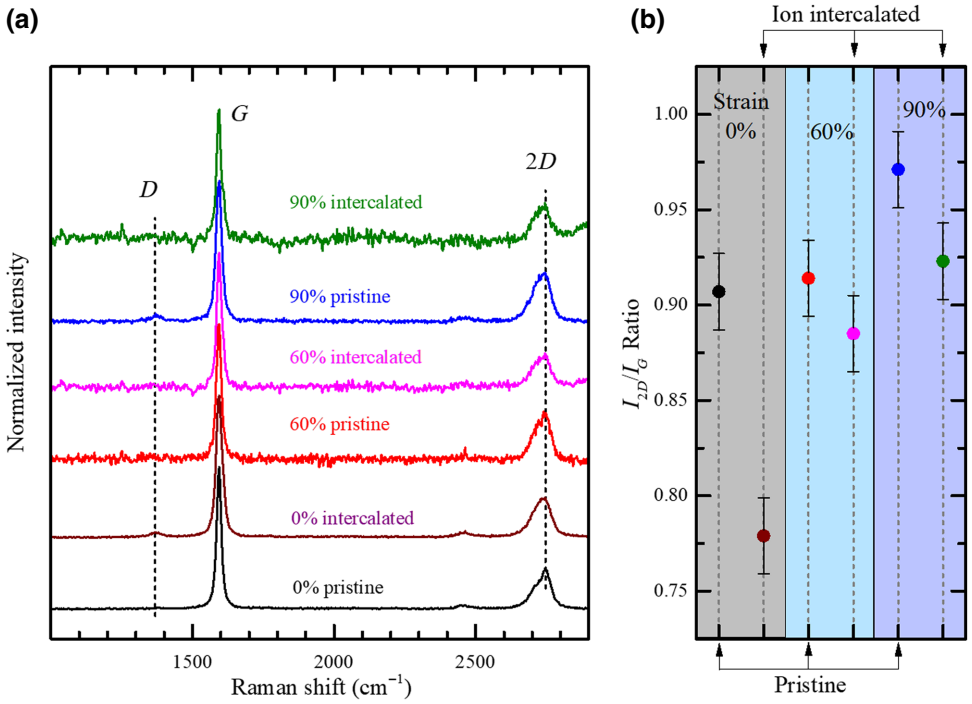

FIG. 4. (a) Raman spectra of GA with 0%, 60%, and 90% strain before and after ion intercalation. Note that the spectra are normalized to [0, 1] and shifted vertically for better comparison. (b) Spectral intensity ratio of 2*D* and *G* features for samples before and after ion intercalation.

and 2*D* around 2740 cm^{-1}, which suggests a sample with high crystallinity [25]. Neither compression nor ion intercalation leads to much increase in spectral intensity around 1370 cm^{-1}, which is associated with *D* band, activated by defects in the double-resonance Raman scattering [26]. Therefore, the structure of GAs at the atomic level remains relatively unchanged upon compression and ion intercalation.

Interestingly, the intensity ratio between 2*D* and *G* features (I_{2D}/I_G) increases with increasing strain. Since the 2*D* feature originates from the overtone of in-plane transverse optical phonons around the *K* point and is activated by triple-resonance Raman scattering, its intensity and shape are sensitive to the stacking order of graphene layers, defects, and strain [26]. The evolution of the 2*D* feature suggests that there is higher structural order in GA after compression [14], which is consistent with the XRD observations.

Furthermore, the I_{2D}/I_G ratio decreases after ion intercalation. Since there is no significant *D* feature presence in the Raman spectra, the change in I_{2D}/I_G is not likely due to an increase of defect density. It should be pointed out that the 2*D* feature is contributed by both electron-phonon and electron-electron scattering. For a low doping level, the electron-electron scattering is sensitive to the charge carrier concentration [27]. Therefore, the decrease of I_{2D}/I_G indicates an increase in doping level, which is consistent with observations of change in sheet resistance (Supplemental Material, Sec. S2 [20]) and emissivity of GA [Fig. 1(c)].

Unlike other graphene-based materials (e.g., MLG), the porous structure of GA makes it easier for ILs to transport in the electrode, and offers better resilience to ion intercalation (e.g., resulting in less structural damage). Furthermore, the charges can be transferred to carbons not only from anions intercalated into graphene layers, but also from anions adsorbed on the three-dimensional network structures formed by MLG in GA. Therefore, the device lifetime is greatly improved, while a comparable modulation depth is obtained. Based on the comparison of GA with and without strain, a moderate strain is beneficial for providing sufficient area for anions in ILs to access carbons in GA, without introducing excessive resisting force induced by capillary pressure.

IV. CONCLUSION

This study demonstrates that the emissivity of GA can be tuned through ion intercalation by electrostatic gating. Moreover, the excellent elastic properties of GA offer an additional dimension (i.e., tuning strain) in modulating emissivity. A comparison study of GA with different stains suggests that a moderate compressive strain provides the best performance in dynamically controlling the emissivity of GA, which is comparable with or superior to other graphene-based materials (e.g., MLG) in terms

of the modulation depth and device lifetime. The easiness of large-scale production of GA at low cost makes it a promising candidate as an electrode in infrared emissivity modulators.

ACKNOWLEDGMENTS

This study is financially supported by the Natural Science Foundation of China (Grants No. 11874423 and No. 12174321).

CONFLICT OF INTEREST

The authors declare that they have no known competing financial interests or personal relationships that could have appeared to influence the work reported in this paper.

AUTHOR CONTRIBUTIONS

Z.W. prepared and characterized the modulator. H.K. performed the data analysis. X.G. and S.C. prepared the materials. T.L., W.P., M.D., and W.C. supported the investigation. Y.Z. drafted the manuscript. X.Z. conceived the idea for the project. All authors participated in discussions of the research, and have given approval to the final version of the manuscript. Z.W. and H.K. contributed equally to this study.

DATA AVAILABILITY

The data that support the findings of this study are available from the corresponding authors upon reasonable request.

[1] B. Zhao, M. Hu, X. Ao, N. Chen, and G. Pei, Radiative cooling: A review of fundamentals, materials, applications, and prospects, Appl. Energy **236**, 489 (2019).

[2] S. Ishii, T. D. Dao, and T. Nagao, Radiative cooling for continuous thermoelectric power generation in day and night, Appl. Phys. Lett. **117**, 013901 (2020).

[3] Y. Sun, Y. Y. Wang, C. Zhan, S. Chen, H. C. Chang, N. Guo, J. K. Liu, Y. Jia, L. Wang, Y. D. Weng, *et al.*, Flexible mid-infrared radiation modulator with multilayer graphene thin film by ionic liquid gating, ACS Appl. Mater. Interfaces **11**, 13538 (2019).

[4] J. Mandal, Y. K. Fu, A. C. Overvig, M. X. Jia, K. R. Sun, N. N. Shi, H. Zhou, X. H. Xiao, N. F. Yu, and Y. Yang, Hierarchically porous polymer coatings for highly efficient passive daytime radiative cooling, Science **362**, 315 (2018).

[5] T. Li, Y. Zhai, S. M. He, W. T. Gan, Z. Y. Wei, M. Heidarinejad, D. Dalgo, R. Y. Mi, X. P. Zhao, J. W. Song, *et al.*, A radiative cooling structural material, Science **364**, 760 (2019).

[6] S. Chandra, D. Franklin, J. Cozart, A. Safaei, and D. Chanda, Adaptive multispectral infrared camouflage, ACS Photonics **5**, 4513 (2018).

[7] Y. Qu, Q. Li, L. Cai, M. Pan, P. Ghosh, K. Du, and M. Qiu, Thermal camouflage based on the phase-changing material GST, Light: Sci. Appl. **7**, 26 (2018).

[8] A. Krishna, J. M. Kim, J. Leem, M. C. Wang, S. Nam, and J. Lee, Ultraviolet to mid-infrared emissivity control by mechanically reconfigurable graphene, Nano Lett. **19**, 5086 (2019).

[9] C. Xu, G. T. Stiubianu, and A. A. Gorodetsky, Adaptive infrared-reflecting systems inspired by cephalopods, Science **359**, 1495 (2018).

[10] A. L. Szabo and B. Roy, Extended Hubbard model in undoped and doped monolayer and bilayer graphene: Selection rules and organizing principle among competing orders, Phys. Rev. B **103**, 205135 (2021).

[11] W. Li, B. Chen, C. Meng, W. Fang, Y. Xiao, X. Li, Z. Hu, Y. Xu, L. Tong, H. Wang, *et al.*, Ultrafast all-optical graphene modulator, Nano Lett. **14**, 955 (2014).

[12] G. Wang, M. Yu, and X. Feng, Carbon materials for ion-intercalation involved rechargeable battery technologies, Chem. Soc. Rev. **50**, 2388 (2021).

[13] L. Y. Zhao, R. Y. Zhang, C. Y. Deng, Y. X. Peng, and T. Jiang, Tunable infrared emissivity in multilayer graphene by ionic liquid intercalation, Nanomaterials **9**, 1096 (2019).

[14] H. Huang, J. Li, H. Ke, Y. Du, W. Peng, M. Dai, Y. Zhang, and X.-A. Zhang, Impact of ionic liquids on effectiveness of tuning the emissivity of multilayer graphene, ACS Appl. Mater. Interfaces **13**, 26256 (2021).

[15] M. S. Ergoktas, G. Bakan, P. Steiner, C. Bartlam, Y. Malevich, E. Ozden-Yenigun, G. He, N. Karim, P. Cataldi, M. A. Bissett, *et al.*, Graphene-enabled adaptive infrared textiles, Nano Lett. **20**, 5346 (2020).

[16] G. Cui, Z. Peng, X. Y. Chen, Y. Cheng, L. Lu, S. B. Cao, S. D. Ji, G. X. Qu, L. Zhao, S. K. Wang, *et al.*, Freestanding graphene fabric film for flexible infrared camouflage, Adv. Sci. **9**, 2105004 (2022).

[17] X. Guo, S. Cheng, K. Xu, B. Yan, Y. Li, W. Cai, J. Cai, B. Xu, Y. Zhou, Y. Zhang, *et al.*, Controlling anisotropic thermal properties of graphene aerogel by compressive strain, J. Colloid Interface Sci. **619**, 369 (2022).

[18] X. Guo, S. Cheng, B. Yan, Y. Li, R. Huang, J. Li, W. Cai, Y. Zhang, Y. Zhou, and X.-A. Zhang, Free-standing graphene aerogel with improved through-plane thermal conductivity after being annealed at high temperature, J. Colloid Interface Sci. **608**, 2407 (2022).

[19] Y. Zhang, H. Ke, J. Li, Z. Weng, T. Lin, W. Peng, M. Dai, R. Mu, and X.-A. Zhang, Impact of molecular components on performance of multilayer graphene-based infrared emissivity modulator, Appl. Phys. Lett. **120**, 243504 (2022).

[20] See Supplemental Material at http://link.aps.org/supplemental/10.1103/PhysRevApplied.18.034003 for further details about (Sec. S1) the thermal images of GA with and without strain; (Sec. S2) the change in sheet resistance of GA upon ion intercalation; (Sec. S3) the reversible modulation of emissivity, device lifetime of the modulator, and corresponding video; (Sec. S4) the porosity of GA with various strain; (Sec. S5) the electrochemical surface area of GA with various strain.

[21] O. Salihoglu, H. B. Uzlu, O. Yakar, S. Aas, O. Balci, N. Kakenov, S. Balci, S. Olcum, S. Süzer, and C. Kocabas,

Graphene-based adaptive thermal camouflage, Nano Lett. **18**, 4541 (2018).

[22] P. Connor, J. Schuch, B. Kaiser, and W. Jaegermann, The determination of electrochemical active surface area and specific capacity revisited for the system MnOx as an oxygen evolution catalyst, Z. Phys. Chem. **234**, 979 (2020).

[23] S. Sheng, K. Ye, Y. Gao, K. Zhu, J. Yan, G. Wang, and D. Cao, Simultaneously boosting hydrogen production and ethanol upgrading using a highly-efficient hollow needle-like copper cobalt sulfide as a bifunctional electrocatalyst, J. Colloid Interface Sci. **602**, 325 (2021).

[24] J. Li, W. Peng, H. Huang, H. Ke, Z. Liu, R. Huang, X. Guo, S. Cheng, Y. Zhang, M. Dai, *et al.*, Continuously adjusting infrared emissivity of multilayer graphene using pulse voltage, Appl. Phys. Lett. **121**, 042204 (2022).

[25] H. Murata, K. Nozawa, N. Saitoh, N. Yoshizawa, T. Suemasu, and K. Toko, 350 °C synthesis of high-quality multilayer graphene on an insulator using Ni-induced layer exchange, Appl. Phys. Express **13**, 055502 (2020).

[26] J.-B. Wu, M.-L. Lin, X. Cong, H.-N. Liu, and P.-H. Tan, Raman spectroscopy of graphene-based materials and its applications in related devices, Chem. Soc. Rev. **47**, 1822 (2018).

[27] R. Beams, L. Gustavo Cançado, and L. Novotny, Raman characterization of defects and dopants in graphene, J. Phys.: Condens. Matter **27**, 083002 (2015).